

19 **Abstract**

20 Continued global warming is expected to result in drying of Central America, with
21 projections suggesting a decrease in precipitation. Poor hindcasting of precipitation, however, due
22 in part to spatial and temporal limitations in instrumental data, subjects these projections to
23 considerable uncertainty. Paleoclimate proxy data are therefore critical for understanding regional
24 climate responses during times of global climate reorganization. Here we present two lake-
25 sediment based records of precipitation variability in Guatemala along with a synthesis of Central
26 American hydroclimate records spanning the last millennium (800-2000 CE). The synthesis
27 reveals that regional climate responses have been strikingly heterogeneous, even over relatively
28 short distances. Our analysis further suggests that shifts in the mean position of the Intertropical
29 Convergence Zone, which have been invoked by numerous studies to explain variability in Central
30 American and circum-Caribbean proxy records, cannot alone explain the observed pattern of
31 hydroclimate variability. Instead, interactions between several ocean-atmosphere processes and
32 their disparate influences across variable topography have resulted in complex precipitation
33 responses. These complexities highlight the difficulty of reconstructing past precipitation changes
34 across Central America and point to the need for additional paleo-record development and analysis
35 before the relationships between external forcing and hydroclimate change can be robustly
36 determined. Such efforts should help anchor model-based predictions of future responses to
37 continued global warming.

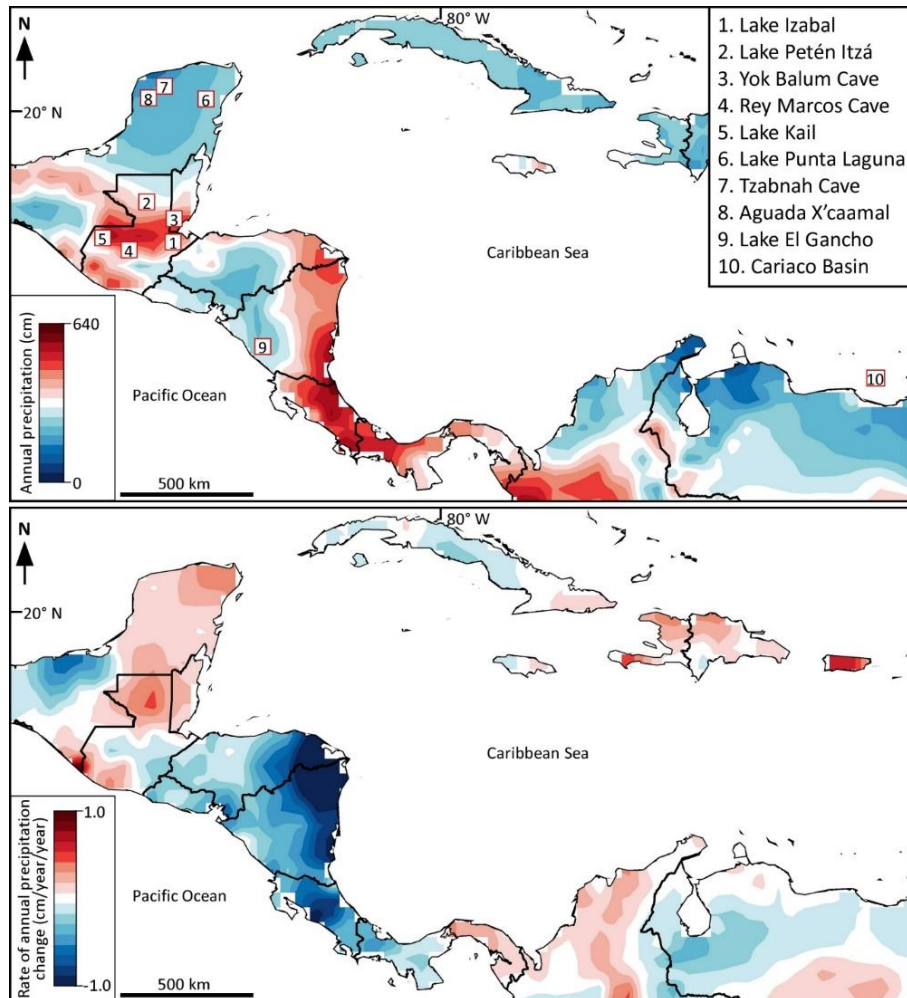
38 **Plain Language Summary**

39 During the last 40 years, Central American precipitation has decreased substantially,
40 creating problems for a region that depends heavily on agriculture. Records suggest, however, that
41 precipitation is not changing uniformly in the region. This differs from climate models that predict
42 uniform drying for the entire Central American region. We set out to investigate Central American
43 climate during the last 1200 years to see if this variability is consistent through time, using
44 precipitation records derived from sediment and speleothems. We acquired two new records from
45 lakes in Guatemala and compare them with existing records from Central America. Our analysis
46 indicates that precipitation has been highly variable across space and time. We suggest that
47 interactions between several atmospheric and oceanic processes produce complex spatiotemporal
48 precipitation variability in the region.

49 **1 Introduction**

50 The last 40 years have been marked by a significant decrease in Central American
51 precipitation (Anderson et al., 2019). Continued global warming will further influence moisture
52 availability in the region (Neelin et al., 2006; Almazroui et al., 2021), potentially through changes
53 in the width, strength and/or position of the Intertropical Convergence Zone (ITCZ; Byrne &
54 Schneider, 2016; Mamalakis et al., 2021). Limitations in regional instrumental data, however, have
55 prevented the robust characterization of precipitation changes in many areas of Central America
56 (CA), and have hindered assessments of climate model hindcasting of precipitation (Imbach et al.,
57 2018). Simulations of future hydroclimate patterns exhibit significant inter-model heterogeneities
58 and fail to replicate the spatially complex precipitation patterns of present day (Christensen et al.,
59 2007; Bhattacharya & Coats, 2020; Fig. 1, Supplementary Figure SF 1), which result from
60 interactions between several ocean-atmosphere processes (Martinez et al., 2019) and steep
61 topographic gradients (Waylen et al., 1996; Imbach et al., 2018). Paleoclimate proxy evidence

62 from Central America is therefore necessary for establishing a long-term perspective on
 63 hydroclimate variability that can inform model hindcasting and future projections.



64 **Figure 1.** Top: Map of Central America, the Caribbean, and northern South America showing mean annual
 65 precipitation based on three gridded data products (Willmott & Matsuura, 2001; Schneider et al., 2011; Harris et al.,
 66 2014) spanning the period 1966-2016 CE. Red squares show the location of proxy records mentioned in the text.
 67 Bottom: Map showing the mean rate of change in annual precipitation over the same time period with the same data.
 68 Note the large gradients in rate of change and mean precipitation in western Central America, especially in the region
 69 where large spatial heterogeneity is observed in the proxy records. For both maps, gridded data was interpolated and
 70 smoothed.

71 A substantial body of evidence points to a change in ITCZ dynamics during the last
 72 millennium, especially during the Little Ice Age (LIA; ~1300 to 1850 CE), when the ITCZ is
 73 hypothesized to have shifted to a more southerly mean position (Haug et al., 2001; Hodell et al.,
 74 2005; Bird et al., 2011). Such an occurrence, were it to be conclusively identified in the paleo-
 75 proxy data, would provide insight on CA hydroclimate responses to a potential future southward
 76 shift in the ITCZ, which some models project should occur as temperatures increase globally
 77 (Christensen et al., 2007; Mamalakis et al., 2021). However, proxy evidence from CA is
 78 inconsistent, pointing to significant spatial variability in hydroclimate during the LIA. For
 79 example, proxy records from the northern Yucatán Peninsula (Hodell et al., 2005) and northern
 80 South America (Haug et al., 2001) indicate regional droughts at this time, suggesting a potential
 81 southward displacement of the rain belt, while proxy records from Belize (Asmerom et al., 2020),

82 the highland regions of Guatemala (Winter et al., 2020; Stansell et al., 2020), and central Mexico
83 (Lozano-García et al., 2007) do not support this pattern, implying a complex regional hydroclimate
84 response that ITCZ dynamics alone cannot explain. These contrasting results suggest that spatial
85 heterogeneity in precipitation variability could be a persistent feature of CA climate on decadal
86 and longer timescales and that synoptic-scale processes, such as changes in ITCZ mean position,
87 can potentially produce incoherent hydroclimate responses across CA.

88 Here we present results from radiocarbon-dated sediment cores obtained from two lakes in
89 the Guatemalan lowlands, Lake Petén Itzá (LPI core) and Lake Izabal (LI core). Our results,
90 combined with a synthesis of proxy records from western CA, show evidence of spatially complex
91 patterns of hydroclimate change during the last millennium, especially during the LIA. We assert
92 that the combination of steep topographic gradients and the interaction between several ocean-
93 atmosphere processes is the reason for the heterogenous pattern of hydroclimate variability. Our
94 analysis suggests that the development of additional paleoclimate records is needed to achieve
95 clarity on how precipitation patterns have varied in CA in response to external forcing and
96 synoptic-scale circulation changes.

97 **2 Study Area and Modern Climatology**

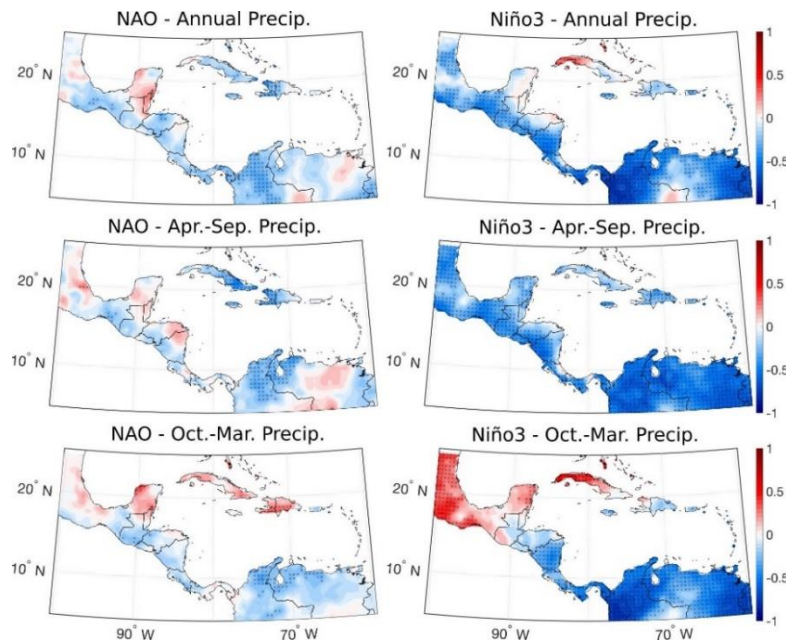
98 Modern precipitation in CA is influenced by the North Atlantic Subtropical High (NASH),
99 the ITCZ, the Caribbean Low-Level Jet (CLLJ), and changes in sea-surface temperatures (SSTs)
100 in both the Pacific and Atlantic basins (Martinez et al., 2019; Fig. 2). The interaction of these
101 ocean-atmosphere processes along with large topographic gradients produces complex spatial
102 patterns of precipitation variability in the region (Fig. 1). For example, due to the high topography
103 along the Caribbean coast of CA, the CLLJ promotes orographic uplift, increasing precipitation in
104 the area (Fig. 1). During the summer, easterly winds bifurcate in the western Caribbean Sea,
105 delivering moisture to the Yucatán Peninsula (Wang, 2007). During the winter, easterly winds
106 shift southward away from the Yucatán Peninsula and across the CA Isthmus towards the Pacific
107 Ocean, reducing precipitation in the Yucatán but, through orographic uplift, increasing
108 precipitation in the highland region of Guatemala (Martinez et al., 2019; Duarte et al., 2021).
109 Disparities between the influence of the CLLJ, the ITCZ, and the NASH, combined with
110 topographic complexities, has resulted in different rates of precipitation change across CA during
111 the last 50 years and in differing precipitation amounts at Izabal and Petén Itzá, with the former
112 receiving around twice as much (~ 3300 mm yr⁻¹ versus ~ 1800 mm yr⁻¹; Fig. 1).

113 Lake Petén Itzá is located in northern Guatemala (Fig. 1), having a surface area of 100 km²,
114 an elevation of ~ 110 m above mean sea level, and a maximum depth of 160 m. The lake water is
115 dominated by bicarbonate and sulfate, calcium, and magnesium ions (Hodell et al., 2008) with
116 minimal river input. Lake Izabal is in the eastern lowlands of Guatemala at ~ 1.5 m above mean
117 sea level, with a surface area of 672 km² and a maximum depth of 15 m. Lake Izabal contains fresh
118 water (Brinson & Nordlie, 1975), and riverine input is significant due to its large catchment (8740
119 km²; Obrist-Farner et al., 2019).

120 3 Materials and Methods

121 2.1 Coring

122 Sediment cores were collected using two piston corers, one for unconsolidated mud-water
 123 interface (MWI) sediments (Fisher et al., 1992) and the other, a modified Livingstone corer, for
 124 deeper, consolidated sediments (Deevey, 1965). The cores were collected during two field seasons
 125 using a wooden platform mounted on two canoes. We collected two sediment cores, one from
 126 Lake Petén Itzá (LPI core; 515 cm long) and one from Lake Izabal (LI core; 455 cm long; Fig. 1).
 127 In Petén Itzá (16°56', 89°55'), the MWI core was collected from the side of the platform to a
 128 sediment depth of 72 cm in 8.4 m of water. The core was extruded in the field at 2.0-cm intervals,
 129 and samples were placed in Whirl-Pak® bags. Next, a PVC casing pipe was lowered through a
 130 hole in the center of the platform and forced into the sediment to a depth of 0.5 cm. Once the casing
 131 was set and cleaned, six core sections were retrieved, to a depth of 515 cm. In Izabal (15°24',
 132 89°16'), the MWI core was collected from the side of the platform to a sediment depth of 55 cm
 133 in 5.7 m of water. The core was extruded in the field at 3.0-cm intervals, and samples were placed
 134 in Whirl-Pak® bags. Next, a PVC casing pipe was lowered through a hole in the center of the
 135 platform and forced into the sediment to a depth of 0.5 m. Once the casing was set and cleaned,
 136 four core sections were retrieved, to a depth of 455 cm. Sediment cores were kept inside the
 137 polycarbonate core barrels and transported to Missouri University of Science and Technology for
 138 further analysis.



139 **Figure 2.** Correlation maps of annual (top), April to September (middle), and October to March (bottom) precipitation
 140 amounts and climate indexes including NAO (left) and Niño3 SSTs (right). Precipitation data are based on three rided
 141 data products spanning 1966-2016 CE (Willmott & Matsuura, 2001; Schneider et al., 2011; Harris et al., 2014). Black
 142 hatches mark regions of significance ($p < 0.1$). Scale bars depict Pearson's r values.

143 2.2 Radiocarbon dating

144 We obtained accelerator mass spectrometry (AMS) radiocarbon dates from both cores
 145 using charcoal and terrestrial wood fragments. Charcoal and wood fragments were washed using

146 deionized water and submitted to the Center for Accelerator Mass Spectrometry at Lawrence
147 Livermore National Laboratory and to the National Ocean Sciences Accelerator Mass
148 Spectrometry (NOSAMS) Facility at Woods Hole Oceanographic Institution. All samples were
149 first treated with a standard acid-base-acid treatment, graphitized, and their radiocarbon
150 concentrations measured via Accelerator Mass Spectrometry. Radiocarbon results were calibrated
151 with OxCal 4.4 (Bronk Ramsey, 2009) using IntCal20 (Reimer et al., 2020). We established age-
152 depth models with the Bayesian software Bacon (Blaauw & Christen, 2011) for the LPI and LI
153 cores (SF2, SF3) using five and seven radiocarbon dates, respectively (ST1, ST2).

154 2.3 Core scans and photographs

155 Cores were scanned using a GEOTEK Multi-sensor core logger at the University of Florida
156 and at LacCore facilities at the University of Minnesota. Cores were first scanned for magnetic
157 susceptibility and density and then opened and split in half to obtain line-scan photographs.
158 Sedimentological observations for both cores were carried out on split core surfaces with the aid
159 of the line-scan photographs (Schnurrenberger et al., 2003). Bed color, sedimentary texture and
160 structure, as well as bedding planes were observed and recorded at 1-cm intervals.

161 The split cores from both locations were analyzed at the Large Lakes Observatory,
162 University of Minnesota, Duluth, USA, using an ITRAX XRF core scanner using a Cr source tube
163 at 30 kV and 55 mA at 5-mm resolution with a 15-second dwell time (SF4, SF5). Raw data were
164 reprocessed to optimize peak-fitting, using QSpec 8.6.0 software (ST3, ST4). In addition, X-
165 radiographs were collected using a Cr source tube run at 60 kV and 30 mA, with variable exposure
166 times, depending on the sediment density. We performed principal component analysis (PCA) in
167 ©MATLAB to investigate the relationship between elements, which allows to represent a
168 multivariate data set as a smaller set of variables to interpret trends or changes in the sediment
169 cores through time. Before PCA analysis, all elemental counts were standardized (converted to z-
170 scores) to avoid confounding effects of dimensional heterogeneity. We utilized the combination
171 of elemental abundances, elemental ratios, and PCA analysis to infer changes in lake catchment
172 and in-lake processes. Elemental ratios discussed in the text are presented on a logarithmic scale
173 due to the asymmetry associated with ratios. Finally, we did not carry out XRF analyses on the
174 upper 50 cm of both cores due to the confounding effects of high water content on XRF analysis
175 (MacLachlan et al., 2015).

176 2.4 Proxy data age-depth modeling and uncertainty analysis

177 We assembled eleven hydroclimate proxy records from lake sediment cores, marine
178 sediment cores, and speleothems, and focused our analysis on 800 to 2000 CE. All proxy records
179 were obtained from the NOAA/World Data Service for Paleoclimatology archives website
180 (<https://www.ncsl.noaa.gov/access/paleo-search/>). For all proxy records, we obtained the
181 published radiocarbon (sediment cores) and U-Th (speleothems) dates and their uncertainties and
182 utilized Bacon (Blaauw & Christen, 2011) to generate age-depth relationships (SF 2, 3, 8-16). For
183 all proxy sites, an additional date was introduced to constrain the most recent year of the record
184 (i.e., the year of sample collection). For the radiocarbon-based age-depth models, we used IntCal20
185 (Reimer et al., 2020) to calibrate the dates. For the Cariaco Basin marine record, we used the
186 published calibrated ages because the radiocarbon ages and the associated uncertainties were not
187 available. For U-Th speleothem models, we used the calibrated U-Th ages and their uncertainties.

188 Bacon (compiled in R) uses the radiocarbon dates and the other age-control points (e.g., date of
 189 core collection or U-Th dates) to model sedimentation rates for sediment cores and growth rates
 190 for speleothems and provides age uncertainty quantification.

191 For the uncertainty analysis, 1000 age-depth pairs were obtained from Bacon, allowing us
 192 to generate 1000 age-proxy pairs for each record. We utilized the 1000 age-proxy pairs and
 193 resampled them at 5-year intervals using a linear interpolation. We used ©MATLAB to assemble
 194 age-model iterations for each proxy site, resulting in a range of proxy values for a specific modeled
 195 age (SF 17-27). We used the 1000 age-proxy pairs and calculated correlation coefficients and
 196 significance (p-values) and report the mean and 1σ for correlation values and the mean p-value.
 197 We used Bretherton's et al. (1999) formula for the effective sample size (ESS) given two time
 198 series X and Y (their equation 30):

$$199 \quad ESS = N \frac{1}{\sum_{i=-(N-1)}^{(N-1)} \left(1 - \frac{|i|}{N}\right) \rho_i^X \rho_i^Y}$$

200 where N is the number of matching samples in both series, and the ρ_i 's are the *i*th-lag
 201 autocorrelation coefficients of the individual time series. This is the more general expression of
 202 their equation 31:

$$203 \quad ESS = N \frac{1 - \rho_1^X \rho_1^Y}{1 + \rho_1^X \rho_1^Y}$$

204 which is only valid when $\rho_1^X, \rho_1^Y \ll 1$.

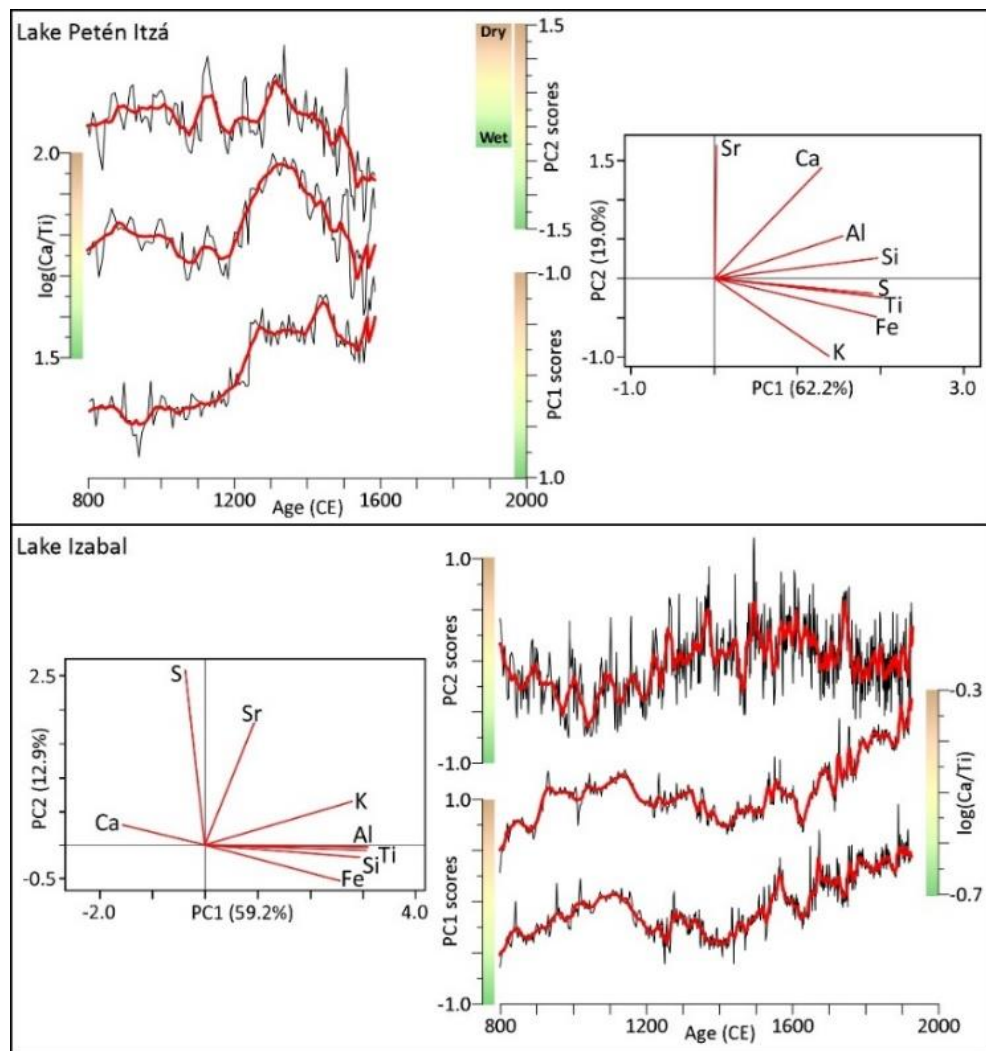
206 3 Results and Interpretations

207 For both studied cores, the ages of the terrestrial wood fragments are in stratigraphic order.
 208 The 515 cm-long LPI core covers the last ~7000 years (Obrist-Farner & Rice, 2019; SF 2, ST 1),
 209 while the 455 cm-long LI core is much shorter, covering the last ~1400 years (Hernández et al.,
 210 2020; SF 3, ST 2). Our results utilize the weighted mean modeled ages for both cores and are
 211 focused on the uppermost 50 to 115 cm (800 to 1585 CE) from the LPI core and on the segment
 212 between 55 and 435 cm (800 to 1926 CE) from the LI core.

213 The 65-cm-long segment of the LPI core is characterized by thinly bedded carbonaceous
 214 mud that alternates in color between dark and light gray (Obrist-Farner & Rice, 2019). The mud
 215 contains variable amounts of gastropod shells and scattered organic debris. PCA analysis of
 216 elemental abundances shows that PC1 predominantly captures variability in terrigenous elements
 217 derived from bedrock erosion (Ti, Al, Fe, K, and Si). The first principal component (PC1) explains
 218 62.2% of the variance in the LPI data (Fig. 3), and we infer that changes in the PC1 score through
 219 time indicate changes in catchment erosion and runoff (e.g., Kylander et al., 2011; Davies et al.,
 220 2015; Duarte et al., 2021). The second principal component (PC2) explains variations related
 221 mostly to Sr and Ca (Fig. 3) and explains an additional 19.0% of the total variance. We infer that
 222 changes in PC2 scores reflect the presence of evaporites, potentially during times of low lake

223 levels, reduced precipitation, and/or increased evaporation (e.g., Mueller et al., 2009; Kylander et
 224 al., 2011; Davies et al., 2015; Fig. 3). Similarly, we utilize the ratio of Ca over Ti as a proxy for
 225 increased evaporation (e.g., Mueller et al., 2009; Kylander et al., 2011; Davies et al., 2015), in
 226 support of our PC2 results.

227 From ~800 to ~1200 CE, elemental abundances from terrigenous elements (e.g., Ti, Al,
 228 and Si) decrease along with PC1 (SF 4, ST 3), indicating reduced catchment erosion for Lake Petén
 229 Itzá (Fig. 3). During this time, there is a slight increase in Ca and S, in PC2 scores, and in the
 230 log(Ca/Ti) ratio. After ~1200 CE, Ti, Al, Si, and K decrease and PC1 scores decline rapidly, while
 231 PC2 scores and the log(Ca/Ti) ratio exhibit a pronounced increase. These results suggest an
 232 increase in evaporation at Lake Petén Itzá that peaked at ~1320 CE. After ~1320 CE, terrigenous
 233 elemental abundance and PC1 scores remain low, and both PC2 scores and the log(Ca/Ti) ratio
 234 decrease toward the uppermost part of the interval, indicating continued low catchment erosion
 235 and a decrease in evaporation.



236 **Figure 3.** Principal component analysis for selected elemental abundances and time series data (black lines) and 10-
 237 point running mean (red lines) showing PC1 scores, log(Ca/Ti), and PC2 scores from lakes Petén Itzá and Izabal. See
 238 SF 4 and SF 5 for additional results.

239 The 400-cm-long segment of the LI core is characterized by homogeneous olive gray silty
240 mud that is faintly laminated and very thinly bedded with minimal organic debris (Hernández et
241 al., 2020). The PCA results show that PC1, which explains 59.2% of the variance, mainly captures
242 variability in Ti, Al, Si, Fe, and K (Fig. 3). We infer that positive PC1 scores indicate an increase
243 in catchment erosion and runoff (e.g., Kylander et al., 2011; Davies et al., 2015; Duarte et al.,
244 2021; Fig. 3). PC2 for the LI core is mostly related to changes in Sr and S and explains 12.9% of
245 the total variance. The processes that PC2 reflect at Lake Izabal are ambiguous because S and Sr
246 in the lake can be related to evaporation, marine water transgression, or redox processes (Duarte
247 et al., 2021; Obrist-Farner et al., 2022).

248 From ~800 to ~1140 CE, there is a decrease in both PC1 and terrigenous elemental
249 abundances, such as Ti, Al, K, and Si (Fig. 3, SF 5, ST 4). Similarly, there is an increase in the
250 $\log(\text{Ca}/\text{Ti})$ ratio and a decrease in PC2 scores. From ~1140 to ~1410 CE, there is an increase in
251 PC1 scores and a decrease in the $\log(\text{Ca}/\text{Ti})$ ratio, while PC2 scores are variable but generally
252 increase. These results suggest a decrease in catchment erosion and runoff in the Lake Izabal area
253 from ~800 to 1140 CE, followed by an increase from 1140 to 1410 CE. After ~1410 CE, PC1
254 scores decrease and the $\log(\text{Ca}/\text{Ti})$ ratio increases, supporting a decrease in catchment erosion and
255 runoff. PC2 scores are highly variable after ~1410 CE.

256 **4 Discussion**

257 There are at least two processes that could potentially explain the spatiotemporal variability
258 in the proxy data from Petén Itzá and Izabal. First, changes in catchment erosion could have
259 resulted from agricultural practices and deforestation in the catchments of both lakes.
260 Paleolimnological investigations in Guatemala and the Yucatán Peninsula have shown that there
261 was a significant increase in catchment erosion during times of increased agricultural activities in
262 the area, especially during the apogee of the Maya civilization (Brenner et al., 2002). Human
263 settlements in the region were at their maximum extent at ~800 CE, resulting in significant erosion,
264 as observed in sediment cores from many Petén lakes (Brenner et al., 2002). The collapse and
265 disintegration of large cities led to rapid forest recovery (Curtis et al., 1998) with a coeval decrease
266 in catchment erosion after ~1000 CE. Our Lake Petén Itza record indicates a decrease in erosion
267 in the area starting at ~1200 CE with a minimum in catchment erosion at ~1350 CE (95% range
268 1230-1420), while the Izabal record indicates an increase in erosion at ~1140 CE with a maximum
269 occurring at ~1410 CE (95% range 1300-1440). Although deforestation and agricultural practices
270 undoubtedly had some influence, it is unlikely that the observed differences in the two records are
271 solely due to these processes.

272 A second possible mechanism for explaining the differences in the Petén Itzá and Izabal
273 records is that the inferred changes in catchment erosion, as well as changes in evaporation,
274 resulted from different hydroclimate patterns at the two locations. For example, the decrease in
275 erosion and increase in evaporation from 800 to ~1100 CE in both records could reflect a decrease
276 in precipitation and increase in evaporation during the well-known Maya droughts (Hodell et al.,
277 1995; Kennett et al., 2012). Between 800 to 1100 CE the two lake records are similar to other
278 paleoclimate datasets from Guatemala, Belize, and the Yucatán Peninsula that suggest a decrease
279 in precipitation at that time (e.g., Douglas et al., 2016). However, after this interval, the records
280 diverge, with the Petén data indicating a decrease in erosion at ~1350 CE and the Izabal record
281 showing a maximum in erosion at ~1410 CE that is highly unlikely to have resulted from human

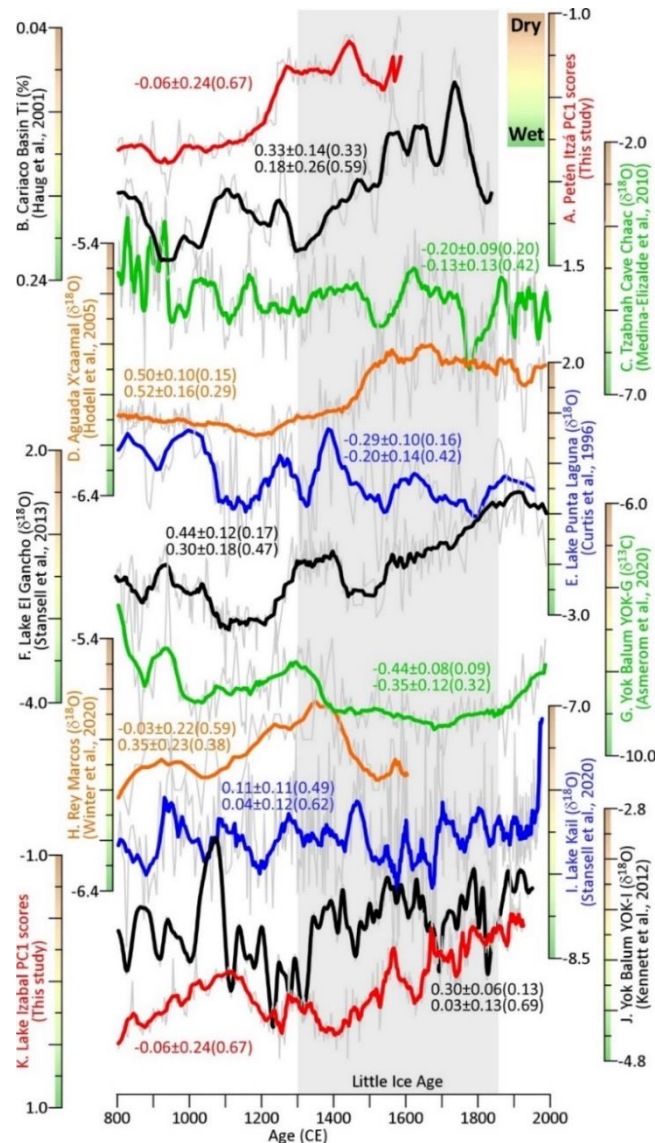
282 disturbance given the known decline in major Mayan population centers well before this time. This
283 difference instead suggests spatially complex and inconsistent hydroclimate in western CA,
284 especially after 1100 CE.

285 Comparison of paleoclimate records from CA reveals that, much like with Izabal and Petén
286 Itzá, inconsistency between records is the norm, even over relatively short distances and especially
287 during the LIA (Figs. 4, 5). Notably, assessment of the relationship between proxy records is made
288 difficult by the uncertainties in radiocarbon and U-Th age-depth models and by the inherent
289 differences in each of the proxy systems. For example, lakes of different sizes and degrees of
290 hydrological closure should be expected to respond differently to changes in hydroclimate, and
291 lake sediment archives from closed-basin settings will not capture the same information as
292 speleothem isotope records, with the former reflecting the balance between evaporation and
293 precipitation and the latter typically reflecting precipitation amount (Hodell et al., 1995; Lachniet,
294 2009). However, the substantial disparities between the proxy records exist even when comparing
295 only speleothem records (SF 6), when comparing records from similar lacustrine systems (SF 7),
296 and when considering age-depth model uncertainties (Figs. 4, 5). For example, the YOK-G
297 speleothem $\delta^{13}\text{C}$ record from Belize (Asmerom et al., 2020; ~70 km north from Izabal) is
298 negatively correlated with Izabal ($r = -0.44 \pm 0.08$; Fig. 5) and indicates wetter than average
299 conditions from ~1400 to ~1850 CE, while both Izabal and the YOK-I speleothem $\delta^{18}\text{O}$ record
300 (Kennett et al., 2012) are positively correlated ($r = 0.30 \pm 0.06$) and indicate peak precipitation at
301 1300-1410 CE and dryer conditions thereafter (Fig. 4). The Yok Balum records themselves exhibit
302 a weak negative correlation ($r = -0.20 \pm 0.05$; Fig. 5), indicating that these two speleothem records
303 from the same cave are not consistent. Additionally, the $\delta^{18}\text{O}$ record from Lake Kail in the western
304 highlands (Stansell et al., 2020; ~250 km west from Izabal) and the Rey Marcos speleothem in the
305 central highlands of Guatemala (Winter et al., 2020; ~100 km west from Izabal) do not exhibit
306 significant correlations with Izabal or Petén Itzá (Figs. 4, 5) and indicate minimal change in
307 precipitation and a reduction in precipitation at ~1350 CE, respectively. The $\delta^{18}\text{O}$ record from
308 Lake Punta Laguna (Curtis et al., 1996) is negatively correlated with Izabal ($r = -0.29 \pm 0.10$) and
309 Petén Itzá ($r = 0.20 \pm 0.14$; Figs. 4, 5) and indicates less precipitation between ~1150 and ~1400
310 CE and wetter conditions thereafter. In contrast, the Aguada X'caamal $\delta^{18}\text{O}$ record (Hodell et al.,
311 2005; ~240 km west from Lake Punta Laguna) is positively correlated with Izabal ($r = 0.50 \pm 0.10$)
312 and Petén Itzá ($r = 0.52 \pm 0.16$; Figs. 4, 5) and indicates persistently dry conditions after ~1250
313 CE. The Tzabnah Cave Chaac $\delta^{18}\text{O}$ record from the Yucatán Peninsula (Medina-Elizalde et al.,
314 2010; ~40 km northeast from Aguada X'caamal) is negatively correlated with Izabal ($r = -0.20 \pm$
315 0.09) and Petén Itzá ($r = -0.13 \pm 0.13$) and indicates alternating dry and wet periods during the
316 LIA.

317 Comparison between more distant records also supports our inference of profound
318 hydroclimate heterogeneity in CA. The $\delta^{18}\text{O}$ record from Lake El Gancho in Nicaragua (Stansell
319 et al., 2013) is positively correlated with Izabal ($r = 0.44 \pm 0.12$; Fig. 5) and weakly correlated with
320 Petén Itzá ($r = 0.30 \pm 0.18$; Fig. 5) and indicates one short wet period between ~1400-1550 CE
321 within an overall drying trend (Figs. 4, 5), similar to the observations from the Izabal and the YOK-
322 I speleothem records. The onset of drying inferred from the Izabal record and the Cariaco Basin
323 Ti record (Haug et al., 2001) are similar ($r = 0.33 \pm 0.14$; Fig. 5); however, Petén Itzá indicates a
324 reduction in precipitation at ~1350 CE, ~400 years earlier than the driest time in northern
325 Venezuela (Fig. 4). Out of the 11 proxy records analyzed, only two of 55 cross-correlations are

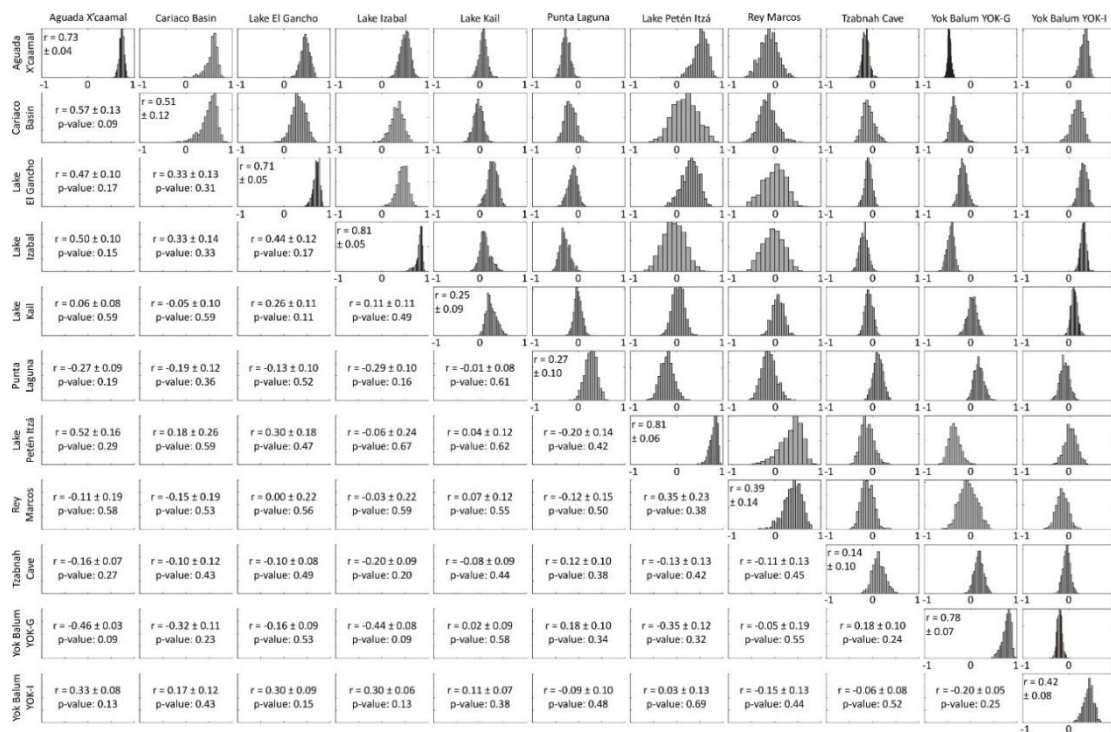
326 statistically significant ($p < 0.1$; Figs. 4, 5; see Supplementary Material), highlighting the
 327 significant inconsistencies in regional hydroclimate proxy records.

328 It is difficult to reconcile the distinct differences in hydroclimate proxy records from CA
 329 by invoking changes in ITCZ dynamics alone. A southward shift in the ITCZ during the LIA (Haug
 330 et al., 2001; Hodell et al., 2005) would have produced persistent regional droughts during boreal
 331 summer if changes in the mean zonal position of the ITCZ were the only factor. Our analysis does
 332 not support this inference, indicating that other ocean-atmosphere processes as well as local
 333 climate controls related to complex topography must be responsible for the complex, regionally
 334 heterogeneous hydroclimate changes observed in the CA proxy records.



335 **Figure 4.** Proxy time series (gray lines) and 10-point running mean (colored lines) from A) Lake Petén Itzá, B) Cariaco
 336 Basin, C) Chaac speleothem, D) Aguada X'caamal, E) Lake Punta Laguna, F) Lake El Gancho, G) Yok Balum YOK-
 337 G, H) Rey Marcos, I) Lake Kail, J) Yok Balum YOK-I, and K) Lake Izabal. Numbers show mean correlation
 338 coefficient values, 1σ , and p-values (see Figure 5) for the time series versus Izabal (upper numbers) and Petén Itzá
 339 (lower numbers).

340 Asmerom et al. (2020) hypothesized that during the LIA, the ITCZ became wider and
 341 weaker, resulting in a decrease in precipitation in northern Venezuela and in an increase along the
 342 northern flanks of the rain belt. However, the drying trend after the onset of the LIA inferred from
 343 Izabal and the YOK-I speleothem (Fig. 4) does not support this hypothesis. That the ITCZ became
 344 wider/weaker during the LIA also fails to explain how the Petén region could have become drier
 345 at this time, as suggested by the proxy data from Lake Petén Itzá and from Aguada X'caamal. An
 346 alternative hypothesis is that moisture availability in western CA was affected by SST gradients
 347 between the Pacific and Atlantic oceans (Metcalf et al., 2015; Bhattacharya & Coats, 2020)
 348 through changes in the El Niño Southern Oscillation (ENSO) and the North Atlantic Oscillation
 349 (NAO). Modern precipitation analysis indicates that positive ENSO events result in reduced
 350 precipitation across the entire Pacific coast of Central America (Dai & Wigley, 2000), whereas
 351 positive NAO conditions result in an increase in precipitation along the eastern coast of Guatemala,
 352 Belize, and the Yucatán Peninsula (Stansell et al., 2020; Fig. 2). During the beginning of the last
 353 millennium, La Niña-like conditions (Cobb et al., 2003) and a more positive NAO (Mann et al.,
 354 2009) would have produced a wetter climate in both the Pacific coast of Central America and on
 355 the eastern coast of Guatemala, Belize, and the Yucatán Peninsula. In contrast, during the LIA, a
 356 change to El Niño-like conditions and a more negative NAO (Cobb et al., 2003; Mann et al., 2009)



357 would have resulted in a drier climate across almost all of CA. Our proxy record synthesis indicates
 358 a regionally incoherent pattern of hydroclimate change during the last millennium, and especially
 359 during the LIA, that likely was not predominantly controlled by any one of these processes, and
 360 instead suggests that a combination of factors controls hydroclimate patterns in CA on
 361 multidecadal and longer timescales.

362 **Figure 5.** Matrix showing the range of correlation values (upper right) for all proxy record realizations utilizing
 363 1000 age-proxy pairs (see supplementary information). The diagonal quantifies the uncertainties in the age-depth
 364 model; for example, an age-depth model with no uncertainty would have correlation equal to 1. Each distribution
 365 represents how correlated each pair of sets of 1000 age-proxy realizations are to each other (see Supplementary

366 Material). The lower left shows mean correlation values, $\pm 1\sigma$, and mean p-values for the records analyzed. The $\delta^{18}\text{O}$
367 records been multiplied by negative one so that positive correlation indicates consistent behavior between proxy
368 sites.

369 One potential mechanism that could further explain the CA proxy record patterns is a
370 change in the intensity of the CLLJ along with topographic controls on moisture delivery to the
371 region. Expansion of the western edge of the NASH could have resulted in a diversion of the CLLJ,
372 the main source of moisture to western CA (Hastenrath, 1984). A southward shift in the CLLJ,
373 combined with steep topography along the Caribbean coast, would have the potential to produce
374 an increase in precipitation at Izabal through enhanced convergence via orographic uplift along
375 with a reduction in precipitation at Petén Itzá. Alternatively, changes in Caribbean SSTs and the
376 Atlantic Warm Pool could have resulted in an increase in moisture availability (Winter et al., 2020;
377 Duarte et al., 2021) and through orographic uplift, increase precipitation along the Caribbean coast
378 and central highlands of Guatemala. Both mechanisms, however, still do not explain why records
379 in the Yucatán Peninsula and other regions of Guatemala show disparate hydroclimate signals over
380 the last millennium and in particular the LIA (Figs. 4, 5).

381 **5 Conclusions**

382 Our results highlight that interactions between numerous ocean-atmosphere processes,
383 including the CLLJ, NAO, ENSO, and changes in ITCZ dynamics, as well as the effects of
384 topography, make it difficult to understand external forcing impacts on hydroclimate in CA.
385 Modern-day precipitation patterns are also spatially complex, with large differences in
386 precipitation amounts over short distances, especially along the mountain ranges and coasts of CA.
387 The available hydroclimate proxy data do not support a simple explanation for hydroclimate
388 variability during the last millennium, in particular that ITCZ dynamics (i.e., changes in latitudinal
389 mean position, width and/or strength) were the main driver of hydroclimate change in the absence
390 of other major controlling factors. Instead, the proxy data suggest that several processes must have
391 interacted to produce the inferred precipitation patterns across the northern tropical rainbelt.
392 Additional proxy records from previously unexplored regions, such as the highland region and
393 Pacific and Caribbean coasts of CA could help clarify and disentangle the influence of the various
394 ocean-atmosphere circulation mechanisms on CA hydroclimate.

395 **Acknowledgments**

396 We thank Oscar Nuñez, Heidy Garcia, Elmer Tun Pana, Noe Hernandez, and Defensores
397 de la Naturaleza who provided lake access and helped us collect the sediment cores. We thank
398 Anders Noren and Kristina Brady Shannon from the National Lacustrine Core Facility (LacCore)
399 for help with core analyses and Robert Brown at the University of Minnesota-Duluth for help
400 with XRF scanning. This is contribution #12 of the MCTF research group. The authors have no
401 known conflicts of interest.

402 **Data Availability**

403 Data for replicating the results of this study are available as supplementary files.
404 Additional paleoclimate proxy datasets are available at the National Oceanic and Atmospheric

405 Administration National Centers for Environmental Information paleoclimate data repository
 406 (<https://www.ncei.noaa.gov/products/paleoclimatology>).

407 References

- 408 Almazroui, M., Islam, M. N., Saeed, F., Saeed, S., Ismail, M., Ehsan, M. A., et al. (2021).
 409 Projected changes in temperature and precipitation over the United States, Central
 410 America, and the Caribbean in CMIP6 GCMs. *Earth Systems and Environment*, 5(1), 1-
 411 24. <https://doi.org/10.1007/s41748-021-00199-5>
- 412 Anderson, T. G., Anchukaitis, K. J., Pons, D., & Taylor, M. (2019). Multiscale trends and
 413 precipitation extremes in the Central American Midsummer Drought. *Environmental*
 414 *Research Letters*, 14(12), 124016. <http://dx.doi.org/10.1088/1748-9326/ab5023>
- 415 Asmerom, Y., Baldini, J. U. L., Prufer, K. M., Polyak, V. J., Ridley, H. E., Aquino, V. V., et al.
 416 (2020). Intertropical convergence zone variability in the Neotropics during the Common
 417 Era. *Science Advances*, 6(7), eaax3644. <https://doi.org/10.1126/sciadv.aax3644>
- 418 Bhattacharya, T., & Coats, S. (2020). Atlantic-Pacific gradients drive last millennium
 419 hydroclimate variability in Mesoamerica. *Geophysical Research Letters*, 47(13),
 420 e2020GL088061. <https://doi.org/10.1029/2020GL088061>.
- 421 Bird, B. W., Abbott, M. B., Vuille, M., Rodbell, D. T., Stansell, N. D., & Rosenmeier, M. F.
 422 (2011). A 2,300-year-long annually resolved record of the South American summer
 423 monsoon from the Peruvian Andes. *Proceedings of the National Academy of Sciences*,
 424 108(21), 8583. <https://doi.org/10.1073/pnas.1003719108>
- 425 Blaauw, M., & Christen, J. A. (2011). Flexible paleoclimate age-depth models using an
 426 autoregressive gamma process. *Bayesian Anal.*, 6(3), 457-474.
 427 <https://projecteuclid.org/443/euclid.ba/1339616472>
- 428 Brenner, M., Rosenmeier, M. F., Hodell, D. A., & Curtis, J. H. (2002). Paleolimnology of the
 429 Maya lowlands: long-term perspectives on interactions among climate, environment, and
 430 humans. *Ancient Mesoamerica*, 13, 141-157. <https://www.jstor.org/stable/26308050>
- 431 Bretherton, C. S., Widmann, M., Dimnikov, V. P., Wallace, J. M., & Blade, I. (1999). The
 432 effective number of spatial degrees of freedom of a time-varying field. *Journal of*
 433 *Climate*, 12(7), 1990-2009. [https://doi.org/10.1175/1520-0442\(1999\)012<1990:TENOSD>2.0.CO;2](https://doi.org/10.1175/1520-0442(1999)012<1990:TENOSD>2.0.CO;2)
- 434 Brinson, M. M., & Nordlie, F. G. (1975). II. Lakes. 8. Central and South America: Lake Izabal,
 435 Guatemala. *SIL Proceedings, 1922-2010*, 19(2), 1468-1479.
 436 <https://doi.org/10.1080/03680770.1974.11896206>
- 437 Bronk Ramsey, C. (2009). Bayesian analysis of radiocarbon dates. *Radiocarbon*, 51, 337-360.
- 438 Byrne, M. P., & Schneider, T. (2016). Narrowing of the ITCZ in a warming climate: Physical
 439 mechanisms. *Geophysical Research Letters*, 43(21), 11,350-311,357.
 440 <https://doi.org/10.1002/2016GL070396>
- 441 Christensen, J. H., Hewitson, B., Busuioc, A., Chen, A., Gao, X., Held, I., et al. (Eds.). (2007).
 442 *Regional climate projections*. Cambridge: Cambridge University Press.
- 443 Cobb, K. M., Charles, C. D., Cheng, H., & Edwards, R. L. (2003). El Niño/Southern Oscillation
 444 and tropical Pacific climate during the last millennium. *Nature*, 424(6946), 271-276.
 445 <https://doi.org/10.1038/nature01779>
- 446 Curtis, J. H., Brenner, M., Hodell, D. A., Balsler, R. A., Islebe, G. A., & Hooghiemstra, H.
 447 (1998). A multi-proxy study of Holocene environmental change in the Maya Lowlands of
 448

- 449 Peten, Guatemala. *Journal of Paleolimnology*, 19(2), 139-159.
 450 <https://doi.org/10.1023/A:1007968508262>
- 451 Curtis, J. H., Hodell, D. A., & Brenner, M. (1996). Climate variability on the Yucatan Peninsula
 452 (Mexico) during the past 3500 years, and implications for Maya cultural evolution.
 453 *Quaternary Research*, 46(1), 37-47. <https://doi.org/10.1006/qres.1996.0042>
- 454 Dai, A., & Wigley, T. M. L. (2000). Global patterns of ENSO-induced precipitation.
 455 *Geophysical Research Letters*, 27(9), 1283-1286. <https://doi.org/10.1029/1999GL011140>
- 456 Davies, S. J., Lamb, H. F., & Roberts, S. J. (2015). Micro-XRF Core Scanning in
 457 Palaeolimnology: Recent Developments. In I. W. Croudace & R. G. Rothwell (Eds.),
 458 *Micro-XRF Studies of Sediment Cores: Applications of a non-destructive tool for the*
 459 *environmental sciences* (pp. 189-226). Dordrecht: Springer Netherlands.
- 460 Deevey, E. S. (1965). Sampling lake sediments by use of the Livingstone sampler. In B. Kummel
 461 & D. Raup (Eds.), *Handbook of paleontological techniques* (pp. 521-529). San Francisco:
 462 Freeman.
- 463 Douglas, P. M. J., Demarest, A. A., Brenner, M., & Canuto, M. A. (2016). Impacts of climate
 464 change and the collapse of lowland Maya civilization. *Annual Review of Earth and*
 465 *Planetary Sciences*, 44(1), 613-645. <https://doi.org/10.1146/annurev-earth-060115-012512>
- 467 Duarte, E., Obrist-Farner, J., Correa-Metrio, A., & Steinman, B. A. (2021). A progressively
 468 wetter early through middle Holocene climate in the eastern lowlands of Guatemala.
 469 *Earth and Planetary Science Letters*, 561, 116807.
 470 <https://doi.org/10.1016/j.epsl.2021.116807>
- 471 Fisher, M. M., Brenner, M., & Reddy, K. R. (1992). A simple, inexpensive piston corer for
 472 collecting undisturbed sediment/water interface profiles. *Journal of Paleolimnology*, 7(2),
 473 157-161. <https://doi.org/10.1007/BF00196870>
- 474 Harris, I., Jones, P. D., Osborn, T. J., & Lister, D. H. (2014). Updated high-resolution grids of
 475 monthly climatic observations – the CRU TS3.10 Dataset. *International Journal of*
 476 *Climatology*, 34(3), 623-642. <https://doi.org/10.1002/joc.3711>
- 477 Hastenrath, S. (1984). Interannual variability and annual cycle: Mechanisms of circulation and
 478 climate in the tropical Atlantic sector. *Monthly Weather Review*, 112, 1097-1107.
 479 [https://doi.org/10.1175/1520-0493\(1984\)112%3C1097:IVAACM%3E2.0.CO;2](https://doi.org/10.1175/1520-0493(1984)112%3C1097:IVAACM%3E2.0.CO;2)
- 480 Haug, G. H., Hughen, K. A., Sigman, D. M., Peterson, L. C., & Röhl, U. (2001). Southward
 481 migration of the Intertropical Convergence Zone through the Holocene. *Science*,
 482 293(5533), 1304. <https://doi.org/10.1126/science.1059725>
- 483 Hernández, E., Obrist-Farner, J., Brenner, M., Kenney, W. F., Curtis, J. H., & Duarte, E. (2020).
 484 Natural and anthropogenic sources of lead, zinc, and nickel in sediments of Lake Izabal,
 485 Guatemala. *Journal of Environmental Sciences*, 96, 117-126.
 486 <https://doi.org/10.1016/j.jes.2020.04.020>
- 487 Hodell, D. A., Anselmetti, F. S., Ariztegui, D., Brenner, M., Curtis, J. H., Gilli, A., et al. (2008).
 488 An 85-ka record of climate change in lowland Central America. *Quaternary Science*
 489 *Reviews*, 27(11-12), 1152-1165. <https://doi.org/10.1016/j.quascirev.2008.02.008>
- 490 Hodell, D. A., Brenner, M., Curtis, J. H., Medina-González, R., Ildefonso-Chan Can, E.,
 491 Albornaz-Pat, A., & Guilderson, T. P. (2005). Climate change on the Yucatan Peninsula
 492 during the Little Ice Age. *Quaternary Research*, 63(2), 109-121.
 493 <https://doi.org/10.1016/j.yqres.2004.11.004>

- 494 Hodell, D. A., Curtis, J. H., & Brenner, M. (1995). Possible role of climate in the collapse of
 495 Classic Maya civilization. *Nature*, 375, 391-394. <https://doi.org/10.1038/375391a0>
- 496 Imbach, P., Chou, S. C., Lyra, A., Rodrigues, D., Rodriguez, D., Latinovic, D., et al. (2018).
 497 Future climate change scenarios in Central America at high spatial resolution. *PLOS*
 498 *ONE*, 13(4), e0193570. <https://doi.org/10.1371/journal.pone.0193570>
- 499 Kennett, D. J., Breitenbach, S. F. M., Aquino, V. V., Asmerom, Y., Awe, J., Baldini, J. U. L., et
 500 al. (2012). Development and disintegration of Maya political systems in response to
 501 climate change. *Science*, 338(6108), 788-791. <https://doi.org/10.1126/science.1226299>
- 502 Kylander, M. E., Ampel, L., Wohlfarth, B., & Veres, D. (2011). High-resolution X-ray
 503 fluorescence core scanning analysis of Les Echets (France) sedimentary sequence: new
 504 insights from chemical proxies. *Journal of Quaternary Science*, 26(1), 109-117.
 505 <https://doi.org/10.1002/jqs.1438>
- 506 Lachniet, M. S. (2009). Climatic and environmental controls on speleothem oxygen-isotope
 507 values. *Quaternary Science Reviews*, 28(5), 412-432.
 508 <https://doi.org/10.1016/j.quascirev.2008.10.021>
- 509 Lozano-García, M. d. S., Caballero, M., Ortega, B., Rodríguez, A., & Sosa, S. (2007). Tracing
 510 the effects of the Little Ice Age in the tropical lowlands of eastern Mesoamerica.
 511 *Proceedings of the National Academy of Sciences*, 104(41), 16200.
 512 <https://doi.org/10.1073/pnas.0707896104>
- 513 MacLachlan, S. E., Hunt, J. E., & Croudace, I. W. (2015). An Empirical Assessment of Variable
 514 Water Content and Grain-Size on X-Ray Fluorescence Core-Scanning Measurements of
 515 Deep Sea Sediments. In I. W. Croudace & R. G. Rothwell (Eds.), *Micro-XRF Studies of*
 516 *Sediment Cores: Applications of a non-destructive tool for the environmental sciences*
 517 (pp. 173-185). Dordrecht: Springer Netherlands.
- 518 Mamalakis, A., Randerson, J. T., Yu, J.-Y., Pritchard, M. S., Magnúsdóttir, G., Smyth, P., et al.
 519 (2021). Zonally contrasting shifts of the tropical rain belt in response to climate change.
 520 *Nature Climate Change*, 11(2), 143-151. <https://doi.org/10.1038/s41558-020-00963-x>
- 521 Mann M., E., Zhang, Z., Rutherford, S., Bradley Raymond, S., Hughes Malcolm, K., Shindell,
 522 D., et al. (2009). Global signatures and dynamical origins of the Little Ice Age and
 523 Medieval Climate Anomaly. *Science*, 326(5957), 1256-1260.
 524 <https://doi.org/10.1126/science.1177303>
- 525 Martinez, C., Goddard, L., Kushnir, Y., & Ting, M. (2019). Seasonal climatology and dynamical
 526 mechanisms of rainfall in the Caribbean. *Climate Dynamics*, 53(1), 825-846.
 527 <https://doi.org/10.1007/s00382-019-04616-4>
- 528 Medina-Elizalde, M., Burns, S. J., Lea, D. W., Asmerom, Y., von Gunten, L., Polyak, V., et al.
 529 (2010). High resolution stalagmite climate record from the Yucatán Peninsula spanning
 530 the Maya terminal classic period. *Earth and Planetary Science Letters*, 298(1), 255-262.
 531 <https://doi.org/10.1016/j.epsl.2010.08.016>
- 532 Metcalfe, S. E., Barron, J. A., & Davies, S. J. (2015). The Holocene history of the North
 533 American Monsoon: ‘known knowns’ and ‘known unknowns’ in understanding its spatial
 534 and temporal complexity. *Quaternary Science Reviews*, 120, 1-27.
 535 <https://doi.org/10.1016/j.quascirev.2015.04.004>
- 536 Mueller, A. D., Islebe, G. A., Hillesheim, M. B., Grzesik, D. A., Anselmetti, F. S., Ariztegui, D.,
 537 et al. (2009). Climate drying and associated forest decline in the lowlands of northern
 538 Guatemala during the late Holocene. *Quaternary Research*, 71(2), 133-141.
 539 <https://doi.org/10.1016/j.yqres.2008.10.002>

- 540 Neelin, J. D., Münnich, M., Su, H., Meyerson, J. E., & Holloway, C. E. (2006). Tropical drying
541 trends in global warming models and observations. *Proceedings of the National Academy*
542 *of Sciences*, 103(16), 6110-6115. <https://doi.org/10.1073/pnas.0601798103>
- 543 Obrist-Farner, J., Brenner, M., Curtis, J. H., Kenney, W. F., & Salvinelli, C. (2019). Recent onset
544 of eutrophication in Lake Izabal, the largest water body in Guatemala. *Journal of*
545 *Paleolimnology*, 62(4), 359-372. <https://doi.org/10.1007/s10933-019-00091-3>
- 546 Obrist-Farner, J., Brenner, M., Stone, J. R., Wojewódka-Przybył, M., Bauersachs, T., Eckert, A.,
547 et al. (2022). New estimates of the magnitude of the sea-level jump during the 8.2 ka
548 event. *Geology*, 50(1), 86-90. <https://doi.org/10.1130/G49296.1>
- 549 Obrist-Farner, J., & Rice, P. M. (2019). Nixtun-Ch'ich' and its environmental impact:
550 Sedimentological and archaeological correlates in a core from Lake Petén Itzá in the
551 southern Maya lowlands, Guatemala. *Journal of Archaeological Science: Reports*, 26,
552 101868. <https://doi.org/10.1016/j.jasrep.2019.05.033>
- 553 Reimer, P. J., Austin, W. E. N., Bard, E., Bayliss, A., Blackwell, P. G., Bronk Ramsey, C., et al.
554 (2020). The IntCal20 Northern Hemisphere radiocarbon age calibration curve (0–55 cal
555 kBP). *Radiocarbon*, 62(4), 725-757. <https://doi.org/10.1017/RDC.2020.41>
- 556 Sachs, J. P., Sachse, D., Smittenberg, R. H., Zhang, Z., Battisti, D. S., & Golubic, S. (2009).
557 Southward movement of the Pacific intertropical convergence zone AD 1400–1850.
558 *Nature Geoscience*, 2(7), 519-525. <https://doi.org/10.1038/ngeo554>
- 559 Schneider, U., Becker, A., Finger, P., Meyer-Christoffer, A., Rudolf, B., & Ziese, M. (2011).
560 *GPCC full data reanalysis version 6.0 at 0.5°: monthly land-surface precipita-tion from*
561 *rain-gauges built on GTS-based and historic data*. Retrieved from:
562 https://doi.org/10.5676/dwd_gpcc/fd_m_v6_050
- 563 Schnurrenberger, D., Russell, J., & Kelts, K. (2003). Classification of lacustrine sediments based
564 on sedimentary components. *Journal of Paleolimnology*, 29(2), 141-154.
565 <https://doi.org/10.1023/A:1023270324800>
- 566 Stansell, N. D., Steinman, B. A., Abbott, M. B., Rubinov, M., & Roman-Lacayo, M. (2013).
567 Lacustrine stable isotope record of precipitation changes in Nicaragua during the Little
568 Ice Age and Medieval Climate Anomaly. *Geology*, 41(2), 151-154.
569 <https://doi.org/10.1130/G33736.1>
- 570 Stansell, N. D., Steinman, B. A., Lachniet, M. S., Feller, J., Harvey, W., Fernandez, A., et al.
571 (2020). A lake sediment stable isotope record of late-middle to late Holocene
572 hydroclimate variability in the western Guatemala highlands. *Earth and Planetary*
573 *Science Letters*, 542, 116327. <https://doi.org/10.1016/j.epsl.2020.116327>
- 574 Wang, C. (2007). Variability of the Caribbean Low-Level Jet and its relations to climate. *Climate*
575 *Dynamics*, 29(4), 411-422. <https://doi.org/10.1007/s00382-007-0243-z>
- 576 Waylen, P. R., Quesada, M. E., & Caviedes, C. N. (1996). Temporal and spatial variability of
577 annual precipitation in Costa Rica and the Southern Oscillation. *International Journal of*
578 *Climatology*, 16(2), 173-193. [https://doi.org/10.1002/\(SICI\)1097-0088\(199602\)16:2<173::AID-JOC12>3.0.CO;2-R](https://doi.org/10.1002/(SICI)1097-0088(199602)16:2<173::AID-JOC12>3.0.CO;2-R)
- 580 Willmott, C. J., & Matsuura, K. (2001). *Terrestrial Air Temperature and Precipitation: Monthly*
581 *and Annual Time Series (1950–1999), Version 5.0.1*. Center for Climatic Research.
582 Retrieved from:
583 http://climate.geog.udel.edu/~climate/html_pages/README.ghcn_ts2.html
- 584 Winter, A., Zanchettin, D., Lachniet, M., Vieten, R., Pausata, F. S. R., Ljungqvist, F. C., et al.
585 (2020). Initiation of a stable convective hydroclimatic regime in Central America circa

586 9000 years BP. *Nature Communications*, 11(1), 716. [https://doi.org/10.1038/s41467-020-](https://doi.org/10.1038/s41467-020-14490-y)
587 [14490-y](https://doi.org/10.1038/s41467-020-14490-y)